

## Supporting Information

### Reagent-adaptive active site switching on $\text{IrO}_x/\text{Ni(OH)}_2$ catalyst

**Qian Zheng,<sup>‡a</sup> Yuandong Yan,<sup>‡a</sup> Jiaying Zhong,<sup>a</sup> Shicheng Yan,<sup>\*a,b</sup> and Zhigang Zou<sup>a,b</sup>**

<sup>a</sup>Collaborative Innovation Center of Advanced Microstructures, National Laboratory of Solid State Microstructures, College of Engineering and Applied Sciences, Nanjing University, No. 22 Hankou Road, Nanjing, Jiangsu 210093, P. R. China.

<sup>b</sup>Jiangsu Key Laboratory for Nano Technology, Eco-materials and Renewable Energy Research Center (ERERC), Nanjing University, No. 22 Hankou Road, Nanjing, Jiangsu 210093, P. R. China

\*Correspondence: [yscfel@nju.edu.cn](mailto:yscfel@nju.edu.cn)

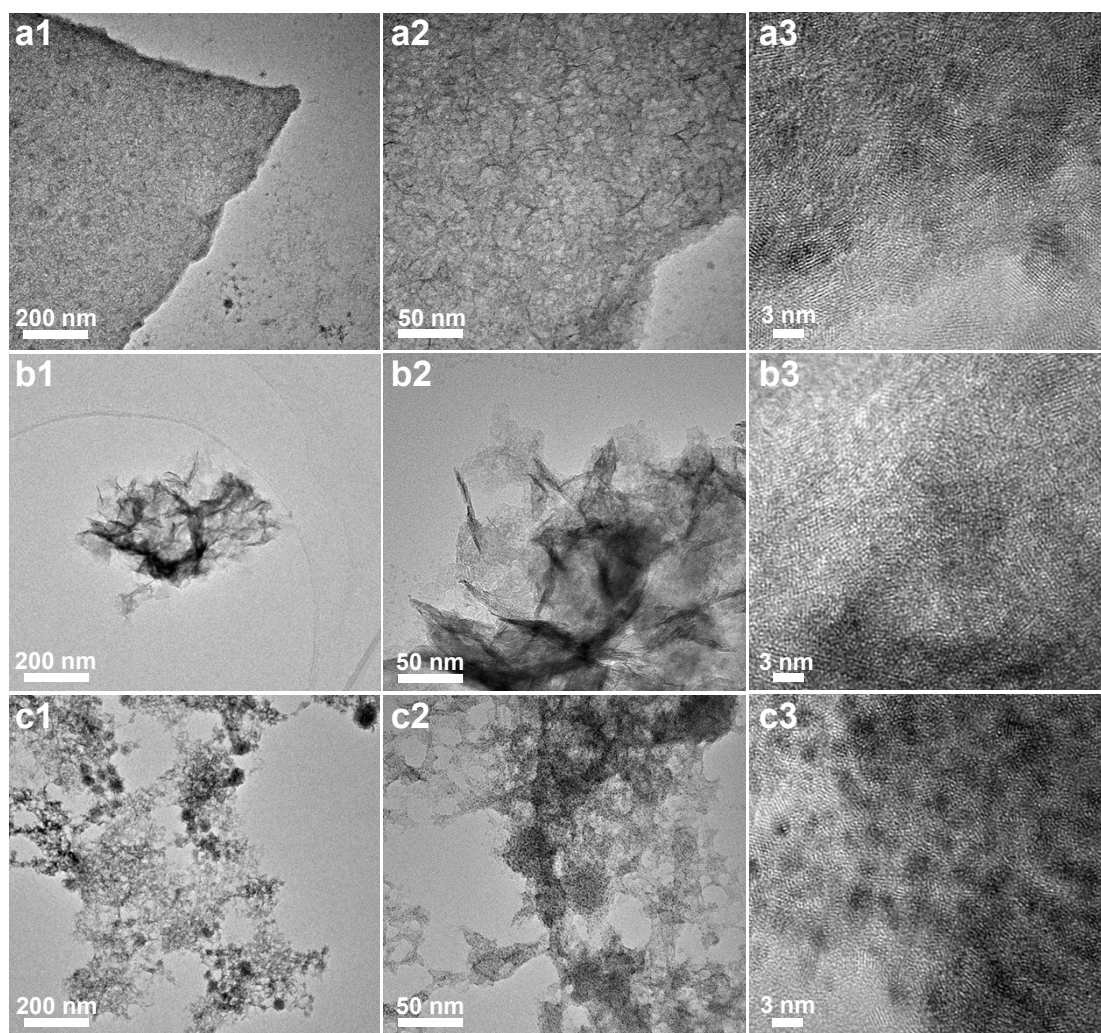


**Fig.S1** The TEM images and high-resolution TEM lattice images of (a1-a3) Ni(OH)<sub>2</sub>, (b1-b3) Ni(OH)<sub>2</sub>-CV, and (c1-c3) IrO<sub>x</sub>/Ni(OH)<sub>2</sub>.

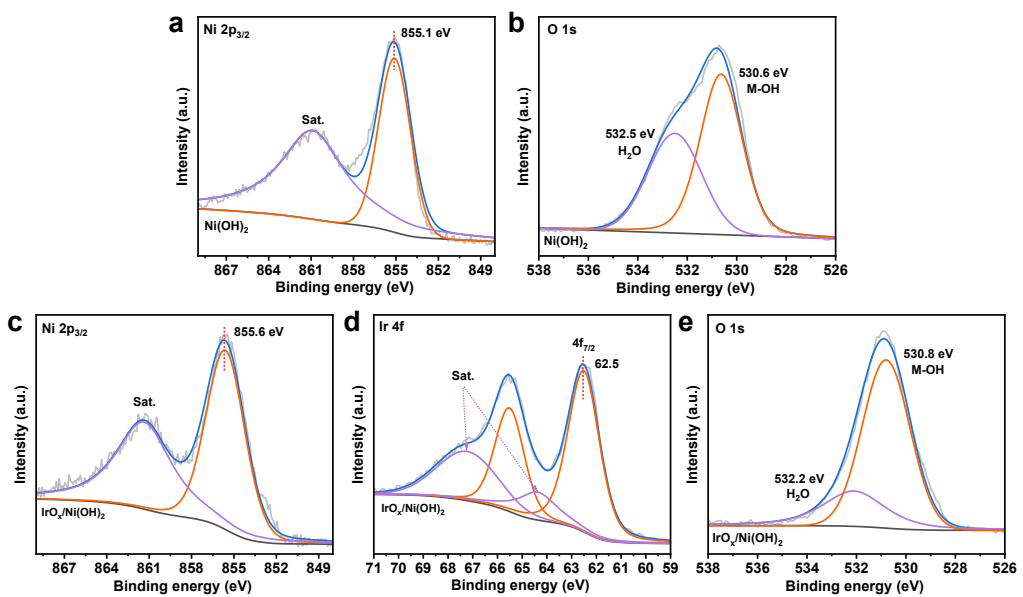


**Fig. S2** (a) Ni 2p<sub>3/2</sub> and (b) O 1s core-level XPS spectra of Ni(OH)<sub>2</sub>. (c) Ni 2p<sub>3/2</sub>, (d) Ir 4f, and (e) O 1s XPS core-level spectra of IrO<sub>x</sub>/Ni(OH)<sub>2</sub>.

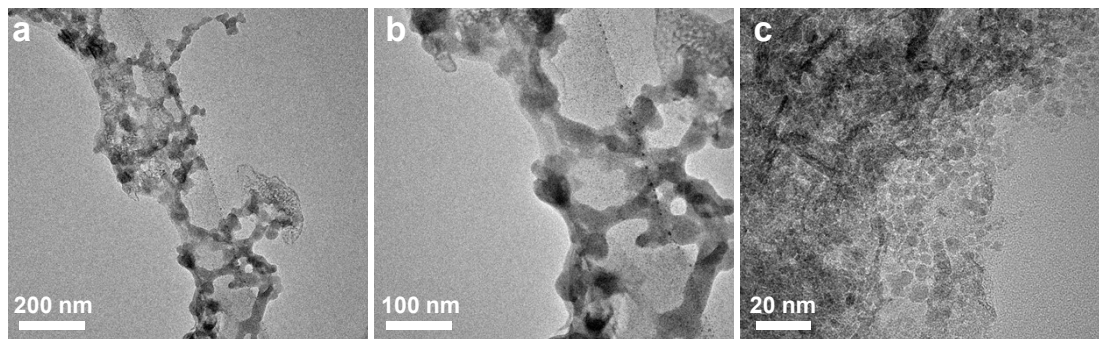


**Fig. S3** The TEM images of electrodepositing  $\text{IrO}_x$  on carbon paper by 200 CV scans in 1 M KOH with  $\text{Ir}^{4+}$ .

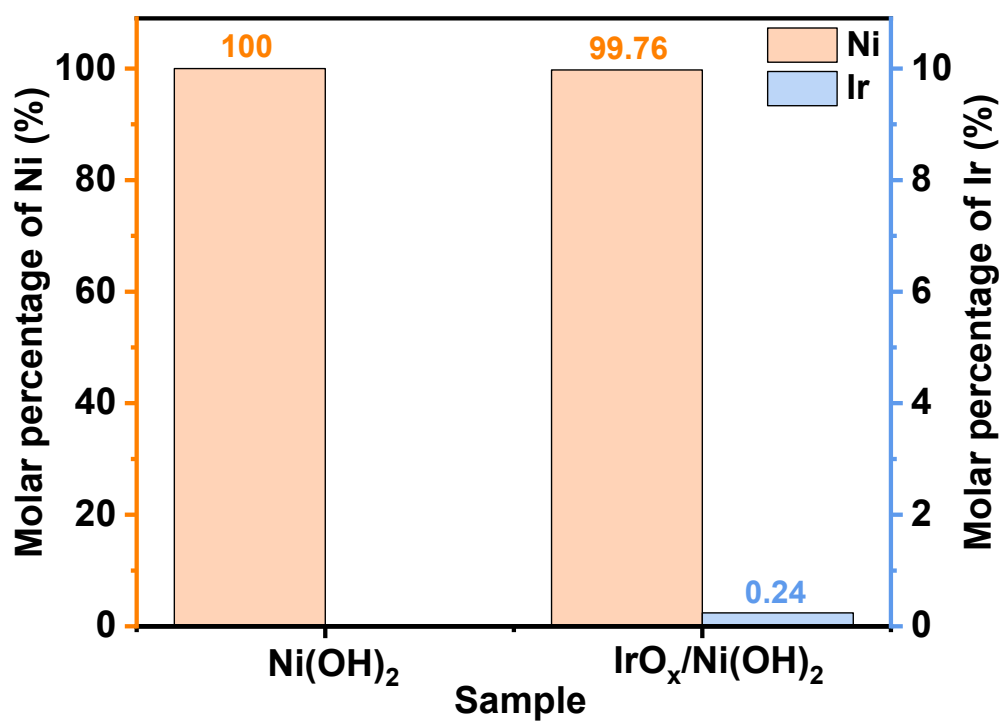
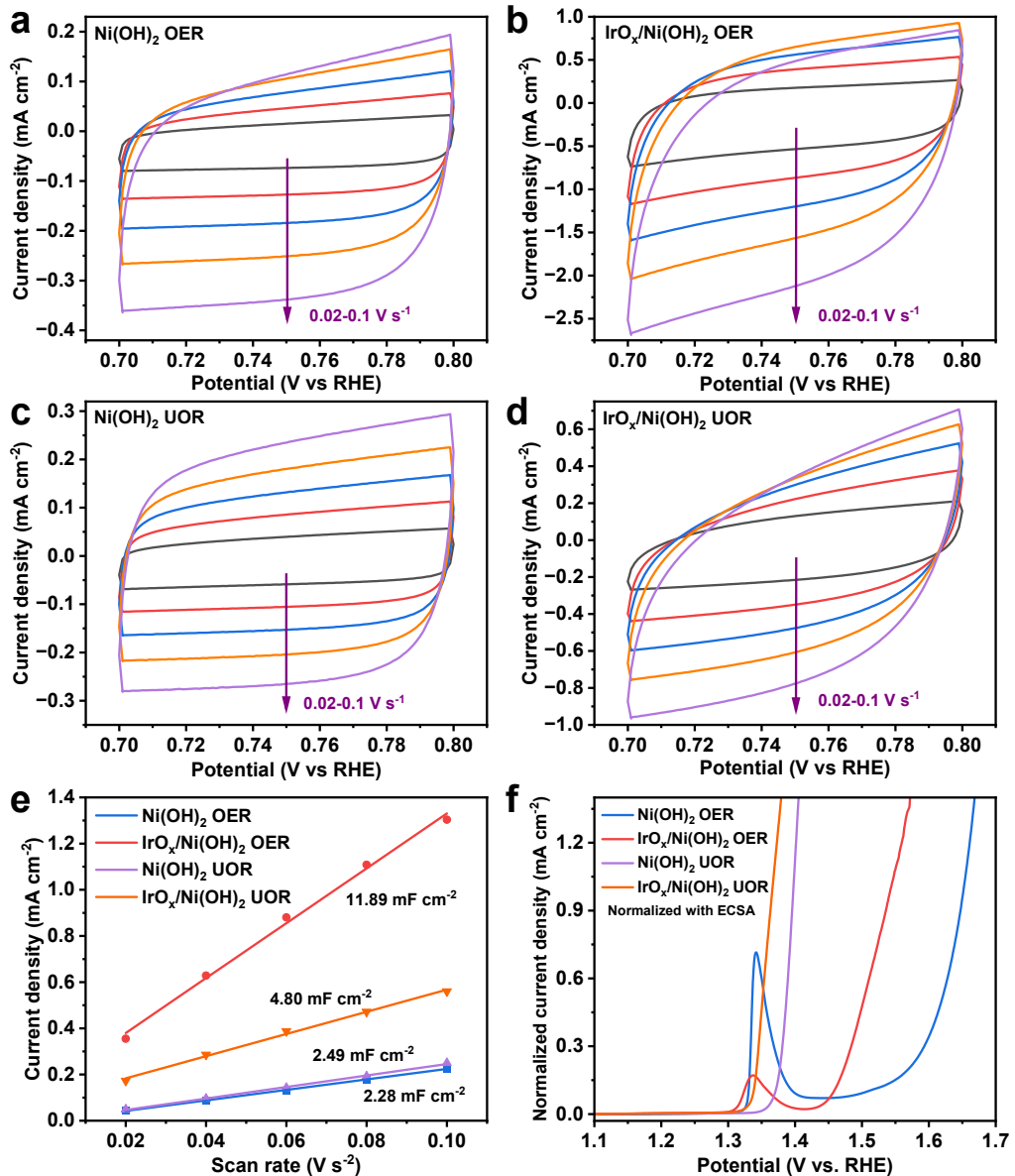
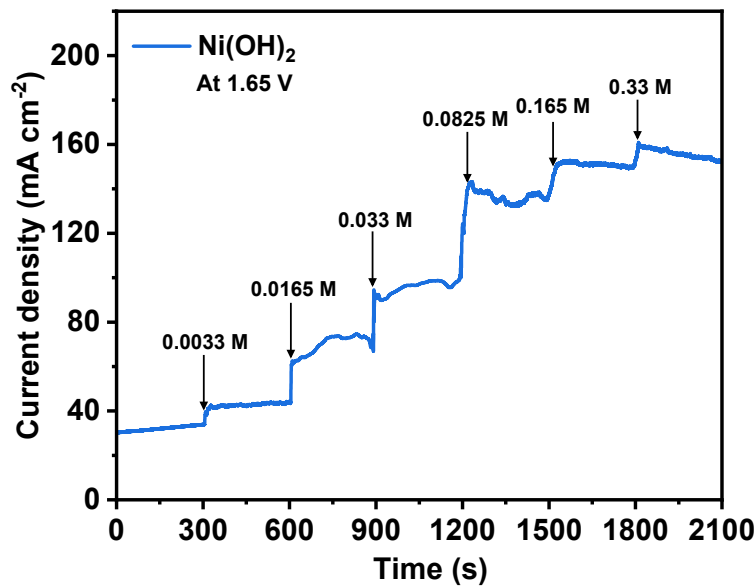


Fig. S4 ICP-AES analysis shows molar percentage of Ni and Ir in  $\text{Ni}(\text{OH})_2$  and  $\text{IrO}_x/\text{Ni}(\text{OH})_2$ .



**Fig. S5** CV scans for (a) Ni(OH)<sub>2</sub> and (b) IrO<sub>x</sub>/Ni(OH)<sub>2</sub> in 1.0 M KOH, and (c) Ni(OH)<sub>2</sub> and (d) IrO<sub>x</sub>/Ni(OH)<sub>2</sub> in 1.0 M KOH + 0.33 M urea. The CV scans were performed in a potential region from 0.7 to 0.8 V vs. RHE and the scan rates range from 0.02 to 0.1 V s<sup>-1</sup>. (e) The linear relationship between the current density and scan rate of the studied electrodes, which is used to calculate the electrochemical active surface area (ECSA). The current density at 0.75 V was used for the calculation of the ECSA. The electrical double-layer capacitance ( $C_{dl}$ ) was calculated by the equation  $C_{dl} = (j_a - j_c)/2v$ , where  $j_a$  and  $j_c$  are the anodic current density and cathodic current density, respectively, and  $v$  is the scan rate. Thus,  $C_{dl}$  is the slope of the linear relationship between  $(j_a - j_c)/2$  and scan rates. The ECSA can be calculated by  $ECSA = C_{dl}/C_{dl,Ref}$ , where  $C_{dl,Ref}$  is the specific capacitance of an ideal flat surface of the catalyst. Here, we use the average value of 0.04 mF cm<sup>-2</sup> for  $C_{dl,Ref}$  in alkaline solutions without taking the used material and measurement conditions into account. (f) LSV curves in Fig.2a-b after normalized by ECSA.



**Fig. S6** The urea concentration-sensitive i-t curve for Ni(OH)<sub>2</sub> electrode at 1.65 V.

The urea-concentration dependent i-t curve of Ni(OH)<sub>2</sub> was recorded at 1.65 V in 1 M KOH +  $x$  M urea ( $0.0033 \leq x \leq 0.33$ ), as shown in **Fig. S6**. Obviously, the current density is closely dependent on the presence of urea, that is, the Ni<sup>3+</sup> oxidizes the urea effectively. This result suggested that the Ni(OH)<sub>2</sub> is an efficient UOR-active catalyst with inefficient water oxidation activity, thus the Ni(OH)<sub>2</sub> electrode without IrO<sub>x</sub> does not have the switching characteristic between UOR and OER.

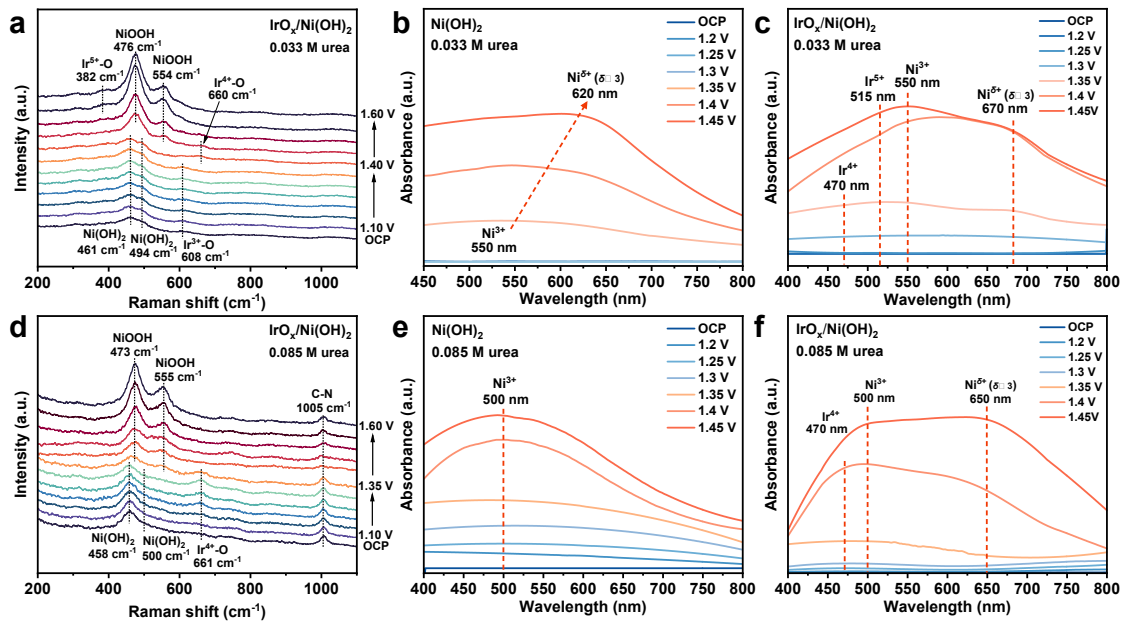


**Fig. S7** Active species on  $\text{IrO}_x/\text{Ni}(\text{OH})_2$ . (a) In situ Raman spectra of  $\text{IrO}_x/\text{Ni}(\text{OH})_2$  in 1 M KOH + 0.033 M urea. The potential increment is 0.05 V when varying potentials from open-circuit potential to 1.6 V. In situ UV-Vis absorption spectra for (b)  $\text{Ni}(\text{OH})_2$  and (c)  $\text{IrO}_x/\text{Ni}(\text{OH})_2$  in 1 M KOH + 0.033 M urea. The potential increment is 0.05 V when varying potentials from open-circuit potential to 1.45 V. (d) In situ Raman spectra of  $\text{IrO}_x/\text{Ni}(\text{OH})_2$  in 1 M KOH + 0.085 M urea. The potential increment is 0.05 V when varying potentials from open-circuit potential to 1.6 V. In situ UV-Vis absorption spectra for (e)  $\text{Ni}(\text{OH})_2$  and (f)  $\text{IrO}_x/\text{Ni}(\text{OH})_2$  in 1 M KOH + 0.085 M urea. The potential increment is 0.05 V when varying potentials from open-circuit potential to 1.45 V.

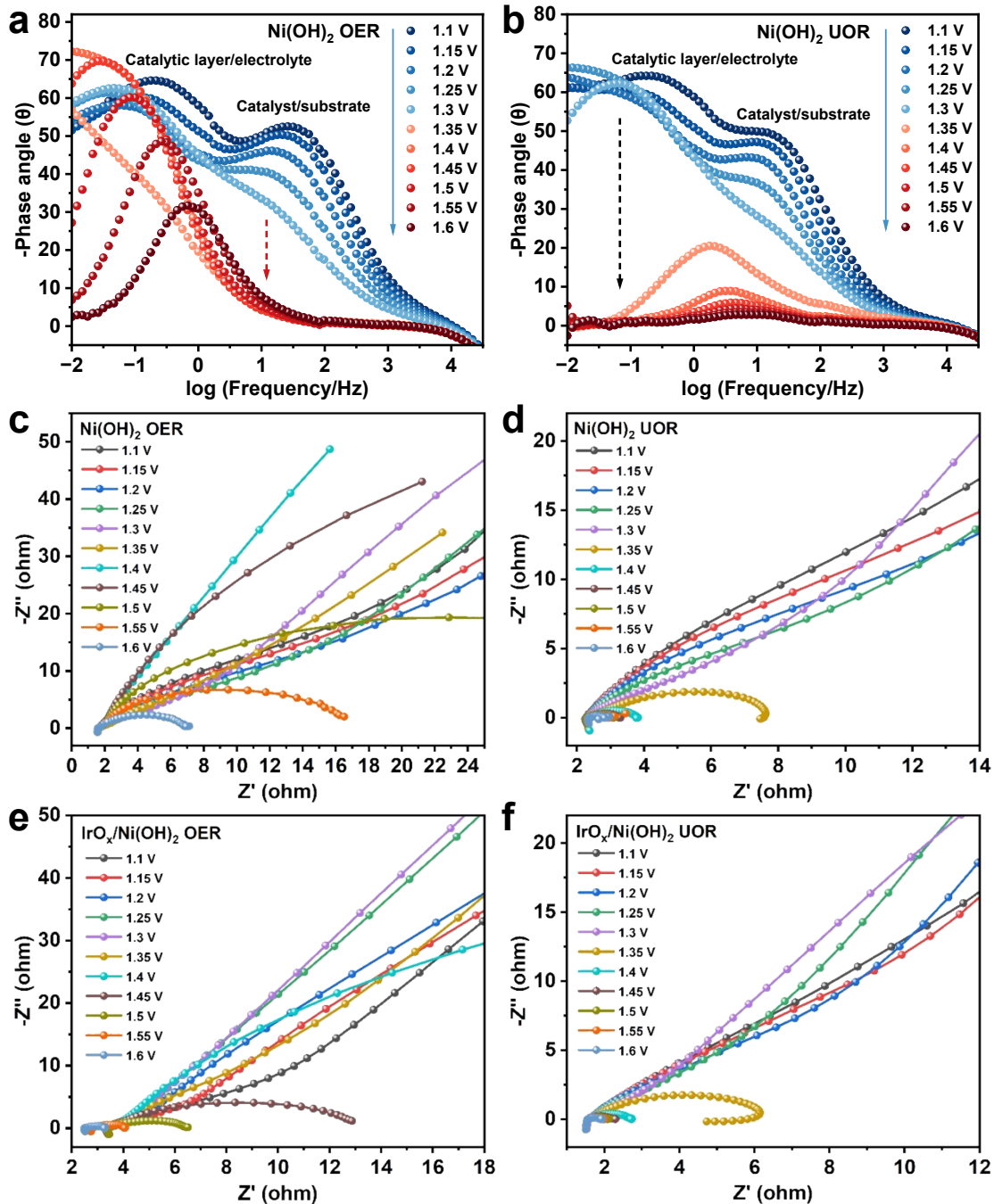


**Fig. S8** Potential-dependent EIS Bode plots of  $\text{Ni(OH)}_2$  electrode when potentials varied from 1.1 to 1.6 V (a) in 1.0 M KOH and (b) in 1.0 M KOH + 0.33 M urea. Potential-dependent Nyquist plots of  $\text{Ni(OH)}_2$  electrode when potentials varied from 1.1 to 1.6 V (c) in 1.0 M KOH and (d) in 1.0 M KOH + 0.33 M urea. Potential-dependent Nyquist plots of  $\text{IrO}_x/\text{Ni(OH)}_2$  electrode when potentials varied from 1.1 to 1.6 V (e) in 1.0 M KOH and (f) in 1.0 M KOH + 0.33 M urea.

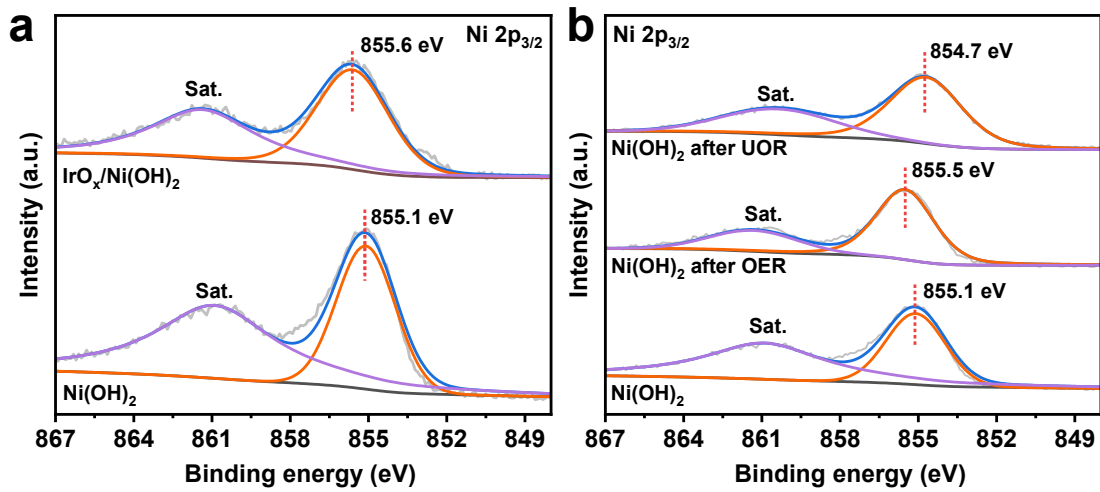


**Fig. S9** (a) Ni 2p<sub>3/2</sub> XPS spectra for Ni(OH)<sub>2</sub> and IrO<sub>x</sub>/Ni(OH)<sub>2</sub>. (b) Ni 2p<sub>3/2</sub> XPS spectra for pristine Ni(OH)<sub>2</sub> and Ni(OH)<sub>2</sub> after OER and UOR.

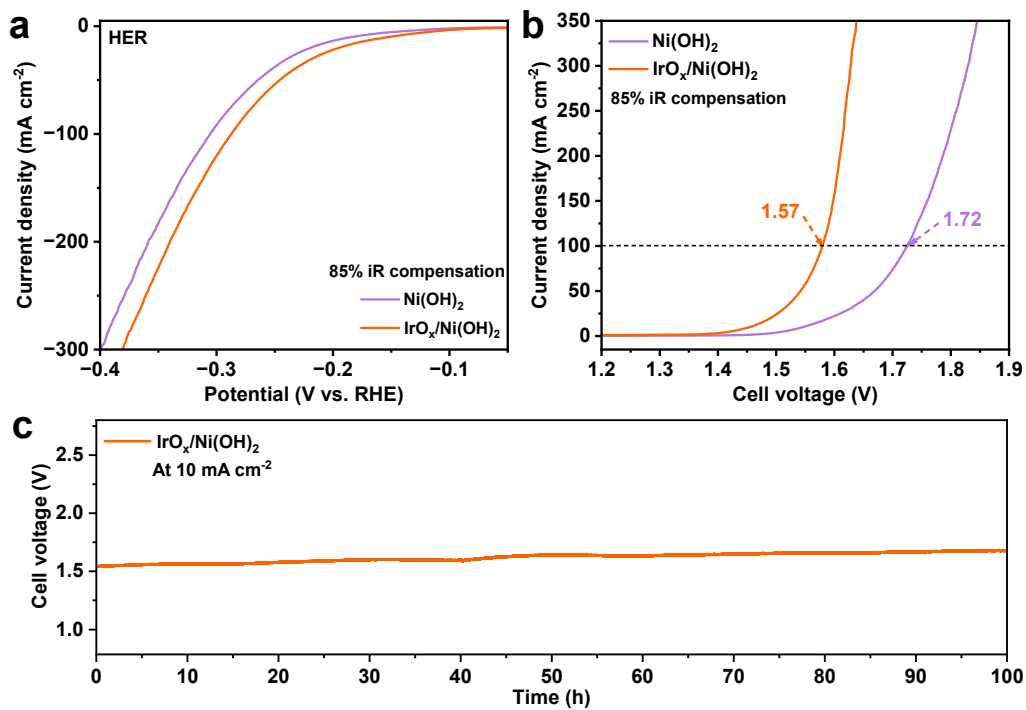


**Fig. S10** (a) LSV curves for HER on Ni(OH)<sub>2</sub> and IrO<sub>x</sub>/Ni(OH)<sub>2</sub> in 1 M KOH. (b) The cell voltage for Ni(OH)<sub>2</sub> electrolyzer and IrO<sub>x</sub>/Ni(OH)<sub>2</sub> electrolyzer in 1 M KOH + 0.33 M urea. (c) The 100 h stability for the IrO<sub>x</sub>/Ni(OH)<sub>2</sub> electrolyzer at 10  $\text{mA cm}^{-2}$  in 1 M KOH + 0.33 M urea.

**Table S1.** The OER and UOR performances on the reported Ni/Ir-based catalysts

Electrocatalyst	Anodic reaction	Overpotential at $10 \text{ mA cm}^{-2}$ (mV)	Electrolyte	References
$\text{IrO}_x/\text{Ni(OH)}_2$	OER	206	1 M KOH	This work
$\text{Ir}/\text{Ni(OH)}_2$	OER	224	1 M KOH	1
$\text{IrNiO}_x/\text{ATO}$	OER	340	0.05 M $\text{H}_2\text{SO}_4$	2
$\text{Ir-Ni}_3\text{N}$	OER	273	1 M KOH	3
$\text{Mn-IrO}_2$	OER	267	1 M KOH	
$\text{Fe-IrO}_2$	OER	300	1 M KOH	
$\text{Co-IrO}_2$	OER	302	1 M KOH	4
$\text{Cr-IrO}_2$	OER	279	1 M KOH	

Electrocatalyst	Anodic reaction	Potential at $10 \text{ mA cm}^{-2}$ (V vs. RHE)	Electrolyte	References
$\text{IrO}_x/\text{Ni(OH)}_2$	UOR	1.337	1 M KOH+0.33 M urea	This work
Nilr	UOR	1.341	1 M KOH+0.5 M urea	5
$\text{Ni}_2\text{P}$	UOR	1.35	1 M KOH+0.5 M urea	6
Ni-Mo	UOR	1.36	1 M KOH+0.1 M urea	7
$\text{Ni}_2\text{P}/\text{Fe}_2\text{P}$	UOR	1.47	1 M KOH+0.5 M urea	8
$\text{Ni-WO}_x$	UOR	1.35	1 M KOH+0.33 M urea	9

**Table S2. Fitting parameters of EIS data for Ni(OH)<sub>2</sub> and IrO<sub>x</sub>/Ni(OH)<sub>2</sub> using the equivalent circuit proposed in Fig. 4d**

	OER (1.55 V)	UOR (1.4 V)		
	Ni(OH) <sub>2</sub>	IrO <sub>x</sub> /Ni(OH) <sub>2</sub>	Ni(OH) <sub>2</sub>	IrO <sub>x</sub> /Ni(OH) <sub>2</sub>
R <sub>s</sub>	1.401	1.675	1.675	1.31
<sup>a</sup> R <sub>1</sub>	10.5	0.448	0.448	0.35
<sup>a</sup> CPE <sub>1</sub> -T	0.287	0.552	0.552	1.186
<sup>a</sup> CPE <sub>1</sub> -P	0.964	0.391	0.391	0.357
<sup>b</sup> R <sub>2</sub>	2.465	1.111	1.111	0.526
<sup>b</sup> CPE <sub>2</sub> -T	0.427	0.083	0.083	0.104
<sup>b</sup> CPE <sub>2</sub> -P	0.643	0.823	0.823	0.897

Notes: <sup>a</sup> The subscript 1 stands for the electron transfer behavior at catalytic layer/electrolyte interface; <sup>b</sup> The subscript 2 indicates the electron transfer behavior at catalyst/substrate interface.

## References

1. Zhao G, Li P, Cheng N, Dou SX, Sun W. An Ir/Ni(OH)<sub>2</sub> heterostructured electrocatalyst for the oxygen evolution reaction: breaking the scaling relation, stabilizing Iridium(V), and beyond. *Adv. Mater.* **32**, 2000872 (2020).
2. Nong HN, et al. Oxide-supported IrNiO<sub>x</sub> core-shell particles as efficient, cost-effective, and stable catalysts for electrochemical water splitting. *Angew. Chem. Int. Ed.* **54**, 2975-2979 (2015).
3. Liu G, Hou F, Wang Y, Wang X, Fang B. Engineering Ir and Ni<sub>3</sub>N heterogeneous interfaces for promoted overall water splitting. *Appl. Surf. Sci.* **637**, 157896 (2023).
4. Lee H, et al. Comparative study of catalytic activities among transition metal-doped IrO<sub>2</sub> nanoparticles. *Sci. Rep.* **8**, 16777 (2018).
5. Xu Y, et al. Ir-doped Ni-based metal-organic framework ultrathin nanosheets on Ni foam for enhanced urea electro-oxidation. *Chem. Commun.* **56**, 2151-2154 (2020).
6. Liu H, Zhu S, Cui Z, Li Z, Wu S, Liang Y. Ni<sub>2</sub>P nanoflakes for the high-performing urea oxidation reaction: linking active sites to a UOR mechanism. *Nanoscale* **13**, 1759-1769 (2021).
7. Zhang JY, et al. Energy-saving hydrogen production coupling urea oxidation over a bifunctional nickel-molybdenum nanotube array. *Nano Energy* **60**, 894-902 (2019).
8. Yan L, et al. Facile in-situ growth of Ni<sub>2</sub>P/Fe<sub>2</sub>P nanohybrids on Ni foam for highly efficient urea electrolysis. *J. Colloid Interface Sci.* **541**, 279-286 (2019).
9. Wang L, et al. Regulating the local charge distribution of Ni active sites for the urea oxidation reaction. *Angew. Chem.* **60**, 10671-10676 (2021).